Eur. Phys. J. D **34**, 291–294 (2005)
DOI: 10.1140/epjd/e2005-00161-2

THE EUROPEAN PHYSICAL JOURNAL D

Growth, structure and electrical properties of tungsten oxide nanorods

M. Gillet[a], R. Delamare, and E. Gillet

Université D'Aix-Marseille III, L2MP-UMR CNRS 6137, Faculté des sciences et techniques, case 151, 52 avenue Escadrille Normandie Niemen, 13397 Marseille Cedex 20, France

Received 6 September 2004
Published online 13 July 2005 –

Abstract. Tungsten trioxide has shown good sensing properties towards various gases. Recently thin nanostructured WO_3 films have been tested. Due to their large surface area to volume ratio they exhibit good sensitivity depending on the grain size. However in conventional WO_3 thin films the average grain size exceeds the thickness of the surface space charge layer, so the electrical conduction is mainly controlled by the carriers transport across the grain boundaries. An alternative way seems to be in a monocrystalline material with nanometric dimensions. Our objective is to fabricate nanosized tungsten oxide rods and to test their sensing properties under gas adsorption. In this work, we focus on the growth, the structure and the electrical properties of tungsten nanorods. The tungsten oxide nanorods were grown by vapour transport from a WO_3 layer onto a substrate (Mica). The nanorods growth was controlled by the temperature gradient between the WO_3 layer and the substrate. Their morphology was investigated by AFM and their structure by TED and TEM. We have investigated the conductivity of the WO_3 nanorods with a technique derived from Atomic Force Microscopy operating in contact mode with a conductive tip (Resiscope).

PACS. 81.10.-h Methods of crystal growth; physics of crystal growth – 61.46.+w Nanoscale materials: clusters, nanoparticles, nanotubes, and nanocrystals – 73.63.-b Electronic transport in nanoscale materials and structures

1 Introduction

Tungsten oxide is a n-type semiconductor with interesting properties in the field of electrochromic devices [1], selective catalyst both for oxidation and reduction reactions [2] and as gas sensors [3–8]. Recently tungsten oxide nanostructured thin films have been tested and have shown superior sensitivity compared with those of bulk materials [7,9–16]. However in thin films the average grain size exceeds the thickness of the surface space charge layer and the electrical transport is largely controlled by the intergrain barrier height. The synthesis of monocrystalline nanostructure is of special interest. More particularly, these structures (called nanorods or nanobelts) are expected to have remarkable electrical properties. Many approaches have been used to prepare nanorods as vapour-liquid-solid growth, solution-liquid-solid methods, template mediate growth, electron beam lithography, scanning tunnelling microscopy techniques and others depending on the expected properties. We have obtained quasi one-dimensional nanostructures in a very simple way using a vapour-solid growth mechanism. We report on the growth mechanism, crystallographic and electrical properties of these nanostructures.

[a] e-mail: marcel.gillet@univ.u-3mrs.fr

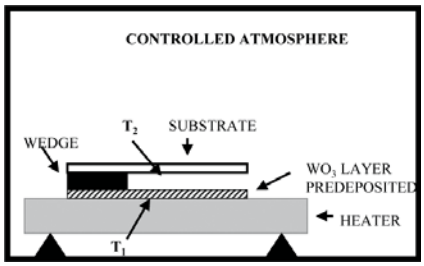

Fig. 1. Experimental set-up of the WO_3 deposition process.

2 Experimental

The tungsten oxide nanostructures are grown by vapour transport in air at atmospheric pressure. The tungsten oxide vapours are produced by a WO_3 layer previously deposited on a SiO_2 slide and condensed onto a mica substrate. The experimental set-up is shown in Figure 1. During the experiments the temperatures T_1 and T_2 determine the supersaturation and the condensation rate. In this work they are maintained at 550 °C and 450 °C respectively. After cooling down to room temperature, the mica substrate with its deposit is examined by Atomic Force Microscopy (AFM). The deposit structure is investigated by Selected Area Electron Diffraction (SAED) and

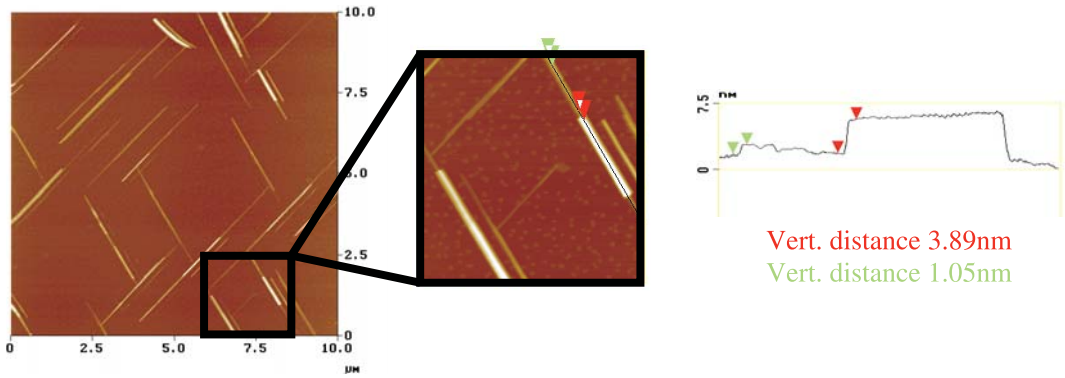

Fig. 2. AFM image of WO_3 nanorods grown on mica (deposition time: 10 min) and a cross-section along a nanorod showing the growth by successive WO_3 monolayers.

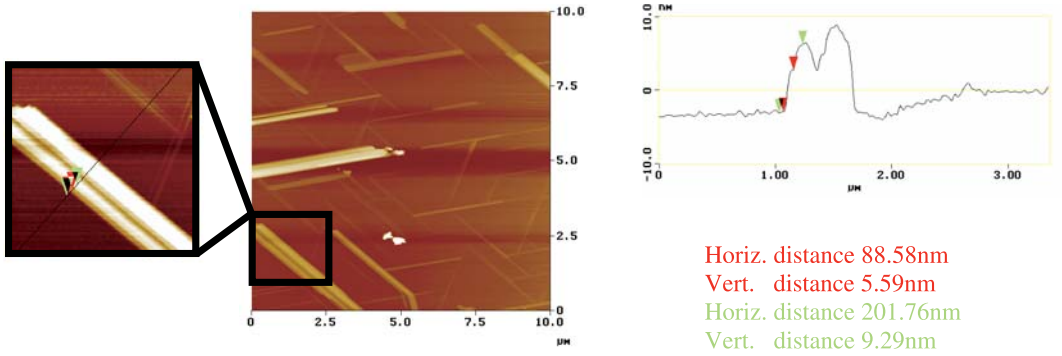

Fig. 3. AFM image of nanorods and nanobelts grown on mica (deposition time: 40 min) and a cross-section of a nanobelt.

Transmission Electron Microscopy (TEM) by means of carbon replica.

3 Results

3.1 Nanostructure morphology

Figures 2 and 3 show nanostructures grown on mica for two different deposition times: 10 mn and 40 mn. Figure 2 shows nanorods with lengths, widths and thicknesses in ranges from 1 to 10 μm, 10 to 200 nm and 1 to 50 nm respectively. The nanostructures in Figure 3 differ from Figure 2 by the fact that the nanorods are composed of some parallel nanorods and some of them exhibit ribbon-like morphology (they are called nanobelts). Nanorods and nanobelts always grow with parallel orientations in two or three directions (1, 2, 3). The orientations 1 and 2 are preponderant. The angles between theses two orientations are 50° and 75°.

3.2 Growth and mechanism

The experimental set-up suggests that the transporting agent is the H_2O vapour and that the growth mechanism depends on the presence of potassium ions on the deposit substrate. It is known that in H_2O vapour at high temperature tungsten oxide may be volatilised through the formation of $WO_2(OH)_2$ according to the reaction [17]:

$$(WO_3) + (H_2O)_g \rightarrow (WO_2(OH)_2)_g. \quad (1)$$

We suppose that $WO_2(OH)_2$ would be condensed on the mica substrate maintained at a relatively low temperature. In the first stage of growth $WO_2(OH)_2$ reacts with the K ions of the mica surface giving a tungsten bronze:

$$WO_2(OH)_2 + xK \rightarrow K_xWO_3 + H_2O. \quad (2)$$

In further growth stage WO_3 is condensed on K_xWO_3. The tungsten bronze forms an intermediate compound between the substrate and the WO_3 nanorods. This interfacial compound is responsible for the nanostructure orientations on the mica substrate.

Assuming that x varies in a range of 0.4 to 0.6 and that the interfacial compound is a tetragonal tungsten bronze with lattice parameters $a = 12.3$ Å and $c = 3.8$ Å [18,19] (Fig. 4 is a representation of the (001) plane). In the (001) plane of the tungsten bronze the next neighbour K atoms distance is 0.47 nm, this value is approximatively the distance between the K ions in the direction [210] on the mica surface. So during the first stage of the growth a tetragonal tungsten bronze is epitaxially formed with good accommodation as indicated in Figure 5. If a_{1s}, a_{2s} and a_{3s} are the distances of K atoms on the mica substrate in the directions [210], [230] and [130] (noted 1, 2, 3 in Fig. 5) respectively and a_d the distance of K atoms in the tetragonal tungsten bronze, the interfacial tungsten

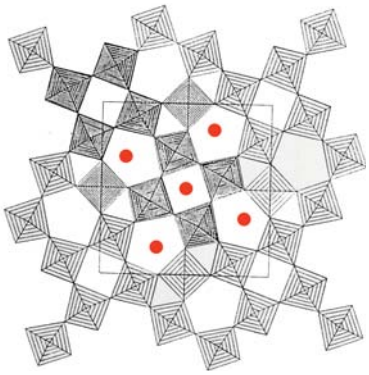

Fig. 4. Schematic representation of (001) plane of the tetragonal tungsten bronze K_xWO_3 ($0.4 < x < 0.6$). $a = 12.3$ Å; $c = 3.8$ Å. ( ) WO_6 octahedrons. ( ) K atoms.

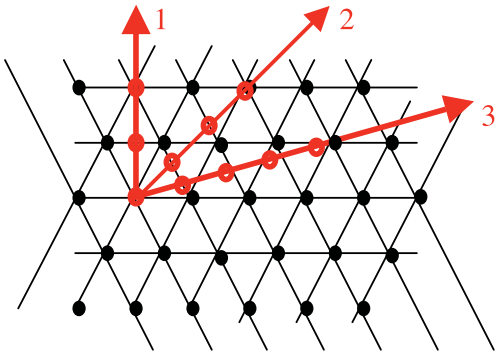

Fig. 5. Representation of the lattice accommodation during the formation of the one-dimensional epitaxial tetragonal tungsten bronze on the mica substrate. Orientation 1: $[210]_{\text{mica}}$ $a_{1s} = 2a_d$; orientation 2: $[230]_{\text{mica}}$ $a_{2s} = 3a_d$; orientation 3: $[130]_{\text{mica}}$ $a_{3s} = 4a_d$. ( ) K atoms on mica substrate, ( ) K atoms in tungsten bronze.

bronze accommodates the substrate with the following relations $a_{1s} = 2a_d$, $a_{2s} = 3a_d$ and $a_{3s} = 4a_d$ according to the three directions 1, 2, 3 so that the angles between the epitaxial orientations are in good agreement with the experimental observations (Fig. 2).

3.3 Structure of the nanorods

The crystallographic structure was investigated by SAED and TEM. Figure 6 is a typical SAED from a nanorod. It shows that the nanorods have a monocrystalline structure. The SAED exhibits two series of diffraction spots. The larger spots are consistent with a monoclinic structure ($a = 7.29$ Å, $b = 7.53$ Å, $c = 7.68$ Å, $\beta = 90.91°$). The nanorods are parallel to the [001] direction and the surface of the nanostructures is parallel to the (100) plane. Weaker diffraction spots evidences a doubling of the parameters. Some nanobelts show evidence for plane defects (twinning and stacking) parallel to the fault axis (Fig. 7) and non-stoichiometric structure $W_{18}O_{49}$ [20].

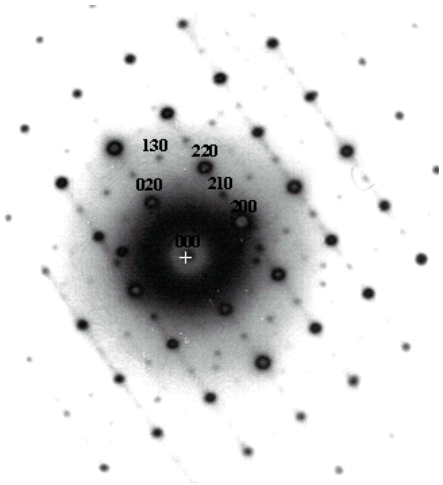

Fig. 6. SAED of a WO_3 nanorod. The strong diffraction spots correspond to a monoclinic structure. Diffusion lines along the direction [010] normal to the nanorod axis are due to the planar defects (microtwins and stacking faults). Additional weak spots indicates a doubling of the parameters.

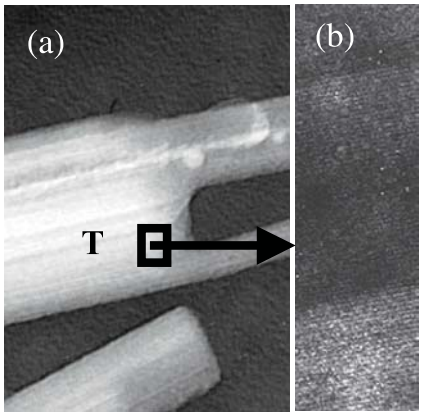

Fig. 7. (a) TEM image of a WO_3 nanorod with planar defects: twinning plane (T) and (b) Stacking faults imaged by HRTEM.

3.4 Electrical properties

The electrical properties of the nanostructure are investigated with a special device attached to an AFM microscope. This device (Resiscope [21]) provides at the same time a classical topographic image of the sample surface and an image representative of the local electrical resistance (or conduction) between the tip and a metallic contact on the substrate. With this technique, we have obtained original electrical data of the WO_3 nanostructures. Figure 8 shows a typical image obtained with the Resiscope. In this case, the resistance is measured between the tip and a gold electrode pre-deposited at the end of a nanorod. As expected, only the nanorod which is connected to the gold electrode has an electrical response and an electrical image. We can note that the resistance increases with the length.

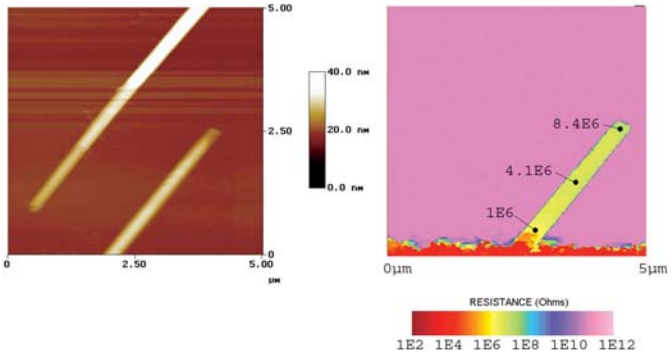

Fig. 8. Topographical image of two nanorods and the corresponding electrical image. The resistance values at three different points of the nanorod on the electrical image are pointed.

4 Summary

A simple method was used to obtain WO_3 nanorods by a vapour-solid mechanism. The nanorods were epitaxially grown on mica at a relatively low temperature. Their morphology was investigated by Atomic Force Microscopy and their structure by Electron Diffraction and Electron Microscopy. Their length, width and thickness are in 1 to 10 μm, 10 to 200 nm and 1 to 50 nm ranges, respectively.

They have a monoclinic structure and grow along the [001] direction, with their (001) plane parallel to the mica substrate. A growth mechanism is proposed with an interfacial tungsten bronze as precursor. The electrical resistance is measured by a device attached to the AFM by means of a conductive tip.

This work is reported by the European contract "Nanostructures for chemical sensors" (Project of the sixth Framework Programme).

References

1. J.S.E.M. Svensson, C.G. Granqvist, Solar Energy Mater. **11**, 29 (1984)
2. F.A. Cotton, G. Wilkinson, *Advances in Organic Chemistry*, 5th edn. (Wiley, New York, 1988), p. 829
3. C. Cantalini, H.T. Sun, M. Faccio, M. Pelino, S. Santucci, L. Lozzi, M. Passacanto, Sensors Actuators B **31**, 81 (1996)
4. M. Akiyama, Z. Zhang, J. Tamaki, M. Miura, N. Yamazoe, T. Harada, Sensors Actuators B **13/14**, 619 (1993)
5. A. Agraval, H. Habibi, Thin Solid Films **169**, 257 (1988)
6. H. Meixner, J. Gerblinger, U. Lampe, M. Fleisher, Sensors Actuators B **23**, 119 (1995)
7. D. Manno, A. Serra, M. Di Giulio, G. Micocci, A. Tepore, Thin Solid Films **324**, 44 (1998)
8. M. Penza, M.A. Tagliente, L. Mirenghi, G. Gerardi, C. Martucci, G. Cassano, Sensors Actuators B **50**, 9 (1998)
9. Zhihong Jin, Huan-Jun Zhou, Zhang-Li Jin, R.F. Savinell, Chung-Chiun Liu, Sensors Actuators B **52**, 188 (1998)
10. E. Liobet, J. Electr. Soc. **147**, 776 (2000)
11. W. Qu, W. Wlodarski, Sensors Actuators B **64**, 42 (2000)
12. C. Cantalini, W. Wlodarski, Y. Li, M. Passacantando, S. Santucci, E. Comini, G. Faglia, G. Sberveglieri, Sensors Actuators B **64**, 182 (2000)
13. L. Lozzi, L. Ottaviano, M. Passacantando, S. Santucci, C. Cantalini, Thin Solid Films **391**, 224 (2001)
14. C. Bittencourt, R. Landers, E. Llobet, G. Molas, X. Correig, M.A.P. Silva, J.E. Sueiras, J. Calderer, J. Electrochem. Soc. **149**, 81 (2002)
15. J. Tamaki, A. Hayashi, Y. Yamamoto, M. Matsuoka, Sensors Actuators B **95**, 111 (2003)
16. S. Wang, Tse-Chuan Chou, Chung-Chiun Liu, Sensors Actuators B **94**, 343 (2003)
17. X. Miao, J. Crystal Growth **197**, 1008 (1999)
18. R. Fan, X.H. Chen, Z. Gui, Z. Sun, S.Y. Li, Z.Y. Chen, J. Phys. Chem. Sol. **61**, 2029 (2000)
19. X.G. Yang, C. Li, M.S. Mo, J.H. Zhan, W.C. Yu, Y. Yan, Y.T. Qian, J. Crystal Growth **249**, 594 (2003)
20. Y.Q. Zhu, W. Hu, W.K. Hsu, D.R.M. Walton, H. Terromes, D.R. Troto, J.F. Hare, D.L. Gobert, Chem. Phys. Lett. **309**, 327 (1999)
21. M. Gadenne, O. Schneegans, F. Houzé, P. Chrétien, C. Demarest, J. Sztern, P. Gadenne, Physica B **279**, 94 (2000)